Nucl Eng Technol 47 (2015) 102–114

Available online at www.sciencedirect.com

ScienceDirect

journal homepage: http://www.journals.elsevier.com/nuclear-engineering-and-technology/

Original Article

TECHNIQUES FOR INTERGRANULAR CRACK FORMATION AND ASSESSMENT IN ALLOY 600 BASE AND ALLOY 182 WELD METALS

TAE HYUN LEE [a], IL SOON HWANG [b], HONG DEOK KIM [c], and JI HYUN KIM [d,*]

[a] Korea Institute of Machinery & Materials (KIMM), 156 Gajeongbuk-Ro, Yuseong-Gu, Daejeon 305-343, Republic of Korea
[b] Department of Nuclear Engineering, Seoul National University, 599 Gwanak-ro, Gwanak-gu, Seoul 151-742, Republic of Korea
[c] Central Research Institute, Korea Hydro and Nuclear Power Co., Ltd, 70 Yuseongdaero, Yusung-gu, Daejon 305-343, Republic of Korea
[d] School of Mechanical and Nuclear Engineering, Ulsan National Institute of Science and Technology (UNIST), 100 Banyeon-ri, Ulju-gun, Ulsan 689-798, Republic of Korea

ARTICLE INFO

Article history:
Received 29 April 2014
Received in revised form
8 August 2014
Accepted 27 August 2014
Available online 21 January 2015

Keywords:
Alloy 182
Alloy 600
Direct current potential drop
Finite-element method
Mock-up crack
Nondestructive examination
Stress corrosion crack

ABSTRACT

Background: A technique developed to produce artificial intergranular stress corrosion cracks in structural components was applied to thick, forged alloy 600 base and alloy 182 weld metals for use in the qualification of nondestructive examination techniques for welded components in nuclear power plants.
Methods: An externally controlled procedure was demonstrated to produce intergranular stress corrosion cracks that are comparable to service-induced cracks in both the base and weld metals. During the process of crack generation, an online direct current potential drop method using array probes was used to measure and monitor the sizes and shapes of the cracks.
Results: A microstructural characterization of the produced cracks revealed realistic conformation of the crack faces unlike those in machined notches produced by an electrodischarge machine or simple fatigue loading using a universal testing machine.
Conclusion: A comparison with a destructive metallographic examination showed that the characteristics, orientations, and sizes of the intergranular cracks produced in this study are highly reproducible.

1. Introduction

Nickel-based alloys and welds between them are widely used as materials for tubes and penetration nozzles for major structural components in pressurized water reactors, such as pressurizer (PZR) instrument nozzles, PZR heater sleeves, steam-generator (SG) drain nozzles, hot-leg instrument nozzles, control-rod drive mechanism nozzles, piping safe ends, and SG tubing, because of their resistance to corrosion and cracking. Recently, however, extensive intergranular stress

* *Corresponding author.*
E-mail address: kimjh@unist.ac.kr (J.H. Kim).

http://dx.doi.org/10.1016/j.net.2014.08.002
1738-5733/Copyright © 2015, Published by Elsevier Korea LLC on behalf of Korean Nuclear Society.

corrosion cracks (IGSCCs) have been reported in the primary and secondary sides of pressure-boundary components [1], and this has become a critical issue for nuclear power plant (NPP) safety.

To assess the integrity of NPP components, nondestructive examination (NDE) has been used to detect defects both during component fabrication and in-service inspection. The reliability of NDE evaluation depends strongly on the capabilities of the NDE equipment, the defect geometries, and the experience of evaluating personnel. An essential requirement for NDE is a good correlation between the behavior of the defects used in the qualification process with that of their real equivalents. Although it is commonly understood that the best correlation is achieved using real defects obtained from used or retired components, techniques for producing cracks by electrical discharge machining have been widely used in NDE qualification tests because of their ease of manufacturing. However, these techniques have issues, such as defects that do not accurately represent those in degraded components in power plants or that have additional alterations induced by surrounding materials, and these issues generally lead to overly optimistic evaluations.

Techniques for the introduction of more realistic flaws have been pursued since 1990, when the demonstration of defect detection using real flaws in the field became a requirement for NDE qualification in the United States and Europe [1]. Recent studies have reported that the reliability of NDE detection strongly depends on the morphology of the crack, including features such as the crack-path opening, the fracture-surface roughness, the nature of the surface oxide, the degree of branching, and the presence of residual stresses, as well as the intrinsic uncertainty of NDE [2–11]. These characteristics of the cracks can significantly alter NDE signal propagation by the reflection, diffraction, transmission, attenuation, and diffusion of ultrasonic energy [12]. Therefore, it is important to simulate the mechanism of crack formation accurately and to understand the key characteristics of both service-induced and artificially generated flaws to determine quantitatively how they affect the NDE signal during inspection.

Unlike fatigue-induced cracks, the sizes of IGSCCs are likely to be underestimated because the degree of crack closure and fracture surface roughness are relatively high compared to those of cracks formed by other mechanisms [5,13]. Therefore, in-service inspection of structural components in NPPs can be effectively achieved with qualification specimens that possess as realistic crack characteristics as possible. In order to characterize and calibrate these key techniques, a number of specimens that have intergranular cracks with mechanical, microstructural, and electrochemical characteristics similar to those found in the field are needed. Recently, an advanced technique was developed for the controlled production of simulated IGSCC mock-ups that possess the mechanical and microstructural features comparable to service-induced cracks in alloy 600 SG tubing, which usually has relatively thin walls [14]. In this study, the above technique is extended to relatively thick forged nickel alloy components, including the alloy 600 base and alloy 182 weld metals of PZR nozzles. The mock-up cracks produced by the extended method were characterized using the on-line direct-current potential drop (DCPD) method with array probes, and compared with the results of a destructive metallographic examination.

2. Materials and methods

Specimens from forged sleeves were prepared by an optimized sensitization heat treatment to produce IGSCCs under corrosive aqueous conditions at room temperature and atmospheric pressure. The DCPD method was used to measure the sizes of the cracks in mockups, and finite element analysis (FEA) was applied to derive the calibration equation, which relates the electrical-potential–drop signal to the crack depth and length. Analytical results were compared with experimental results to evaluate the validity and the applicability of the derived equation, and final characterization of the mock-up crack was performed using destructive metallographic analysis. Fig. 1 shows the flow chart describing the procedure used in this study.

2.1. *Preparation of qualification samples*

Both base metal and weld metal samples were prepared. For the base metal samples, commercial heats of forged alloy 600 sleeves (22.5 mm outer diameter, 3.3 mm thickness) that were produced for use as pressurized water reactor PZR heater nozzles for the Korean Standard Nuclear Power Plant were used. The chemical composition of this material is provided in Table 1. Weld samples were produced using gas tungsten-arc welding and shielded metal-arc welding with alloy 182 filler metals for two forged alloy 600 sleeves with machined V-grooves. The welding procedure was in accordance with the specifications of Doosan Heavy Industries & Construction Co., Ltd. under the provision of the ASME Boiler and Pressure Vessel Code, Section IX.

Specimens of the forged sleeves were prepared using the optimized sensitization heat treatment for generating IGSCCs under corrosive aqueous conditions at room temperature and atmospheric pressure. The sensitization heat treatment was applied to make the materials more susceptible to stress corrosion cracking and, consequently, reduce the time and effort required for mock-up crack production. The conditions for the treatment were optimized on the basis of the results from a double-loop electrochemical potentiokinetic reactivation (EPR) test and a microstructural analysis.

Alloy 600 base metal sleeves were aged using heat treatments at 700°C in a 5% hydrogen and 95% argon atmosphere for intervals of 0.25 hours, 1 hours, 5 hours, and 25 hours. The heat-treatment temperature of 700°C was selected using a modified Huey test. The test was conducted in boiling 25% nitric acid for 24 hours to quantify the sensitization induced by the aging heat treatments according to the procedure of ASTM A262 [4,15]. Because the Huey test measures the amount of metal dissolution resulting from intergranular precipitation and grain-boundary chromium depletion, a larger weight loss is generally considered to indicate a higher degree of sensitization [16]. Double-loop EPR and microstructure analyses were performed, and the results were combined to determine the optimum conditions for sensitization heat treatment.

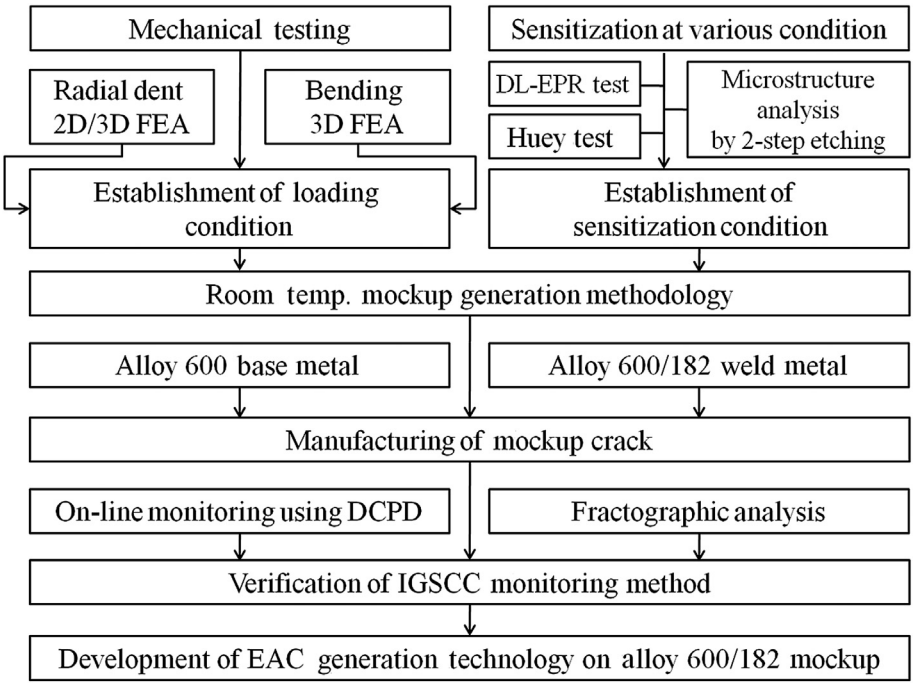

Fig. 1 – Flow chart of the development of mock-up crack generation and validation techniques for Ni-based forged tubes. DCPD, direct-current potential drop; DL-EPR, double-loop electrochemical potentiokinetic reactivation; EAC, environmentally assisted cracking; FEA, finite element analysis; IGSCC, intergranular stress corrosion cracks.

Double-loop EPR tests were conducted on the as-received and heat-treated samples with the same sensitization treatment conditions as those indicated by the Huey test. The test procedure generally conforms to ASTM G108-92. The characteristics of the potential and current measuring instrument were in accordance with ASTM G5-87 over the potential range used (i.e., from −400 mV to + 400 mV on a saturated calomel reference electrode scale) at a scan rate of 0.5 mV/s. A platinum electrode was used as the counter electrode. The 0.01M H_2SO_4 + 0.0001M KSCN test solution was prepared from reagent-grade sulfuric acid (H_2SO_4), potassium thiocyanate (KSCN), and type IV water according to ASTM D-1193. Each test cell contained 500 mL of test solution and the temperature was maintained at 25°C using a controlled-temperature water bath. Prior to each test, the samples were polished to a finish of 1 μm using diamond paste. The samples were then immersed in the test solution until a stable open-circuit potential was achieved. After the EPR tests, chemical etching using an 8:1 solution of orthophosphoric acid and water at a closed circuit potential of 3 V for durations of 15 seconds and 30 seconds was performed to analyze the microstructure of each sample in order to confirm the change in microstructure following heat treatment [16].

Table 1 – Chemical composition of the materials used in this study (in weight %).

Element	Chemical composition	
	Alloy 600	Alloy 182
C	0.054	0.016
Si	0.32	0.13
Mn	0.59	2.21
S	0.005	0.002
Cr	16.3	15.70
Fe	9.82	12.60
Ni	72.4	66.7
Co	0.09	0.01
P	0.008	0.009
Ti	0.208	0.253
Al	0.18	0.22
Nb + Ta	0.025	2.15

The same procedure was applied to the alloy 182 weld metal to establish the optimal sensitization conditions, except for the temperature range and duration of the heat treatment. Postweld heat treatment, which is also known as stress-relief (SR) heat treatment, is generally applied to eliminate residual stresses induced during the welding process. However, there is a possibility of chromium carbide formation along the grain or dendrite boundaries in the alloy 182 region of the weld metal in alloy 600/182 weldments during SR heat treatment, which makes the welds more susceptible to cracking. Tsai et al [17] reported that alloy 182 weld metal was highly sensitized after a heat treatment including solution annealing (SA) at 1,100°C for 24 hours and a SR heat treatment at 620°C for 24 hours. Kubo et al [18] used a SR heat treatment at 615°C for 10 hours and low-temperature heat treatment at 450°C for 200 hours as a sensitization treatment for weld joints of alloy 182 and alloy 82; their results did not show any significant difference between the different treatment conditions. Here, the conditions used by Tsai et al [17] were chosen as the sensitization conditions for the practical generation of weld samples because the sensitization is faster (due to the relatively short heat-treatment time) compared to the conditions used by Kubo et al [18]. While it

is possible that dendritic structures may disappear, and recrystallization may occur, after SA of the weldment, an examination of fracture surface of mock-up crack samples confirmed the existence of dendritic structures in the heat-treated samples from this study. Therefore, a combined heat treatment that comprised SA at 1,100°C for 24 hours followed by water quenching and SR heat treatment at 620°C for 24 hours followed by air cooling was applied to alloy 182 weld. Modified Huey tests were conducted to measure the weight losses of heat-treated alloy 182 welds.

2.2. *Test system setup*

After the optimized sensitization treatment, tensile specimens with a reduced section length of 30 mm and a width of 6.25 mm were prepared from the tubular specimen via electrodischarge machining without disturbing the curvature of the circumference of the sleeve. American Society for Testing and Materials (ASTM) Standard Test Method E8 was followed for testing at room temperature with the loading axis in the axial direction of the tube. Tensile testing of the alloy 600 base metal showed that the ultimate tensile and yield strengths of the as-received specimens are 1050 ± 10 MPa and 490 ± 10 MPa, respectively, while the corresponding values for the sensitization heat-treated specimens are 1030 ± 10 MPa and 485 ± 10 MPa, respectively. From these results, it is apparent that the yield strength is only slightly affected by the sensitization treatment. However, SA heat-treatment of an alloy 182 weld specimen resulted in a significant decrease in the yield strength from 370 ± 10 MPa (in the as-received specimens) to 290 ± 10 MPa because of grain coarsening.

To produce mock-up cracks, a servo-hydraulic materials testing machine with a 100 kN load capacity was used. The stroke, load, and DCPD signals were acquired using a high-speed A/D converter across the main controller. Radial-denting and four-point–bending methods were applied to produce axial and circumferential cracks, respectively, in the tubular specimens. As shown in Fig. 2, the specimen locations that were exposed to a 1M aqueous solution of sodium tetrathionate at room temperature were subsequently compressed by a pair of denting jigs, and DCPD was applied with a probe spacing of about 2 mm. While the DCPD probes were immersed in a test solution, so that they could contact the specimen surface exposed to the test solution, the probe wires and contacts were electrically insulated by PTFE heat shrinkable tubes and microshield paints respectively. The applied compressive load was determined by FEA of the test section, described in below.

To measure the DCPD signals, an Agilent 6671A power supply with a 220 A capacity was employed. The DCPD signals were monitored on-line using an Agilent model 34420A nanomultimeter and an Agilent 3488A switch-control unit. A computer managed the main controller and high-speed A/D converter that were interfaced via General Purpose Interface Bus (GPIB) using the LabView software. A traveling microscope, used for measuring the physical crack length on the outer surface, was attached to the test machine. The DCPD method was applied for the *in situ* monitoring of the initiation and propagation of the crack length and depth. Five pairs of voltage probes were attached at 2 mm intervals across the rectangular

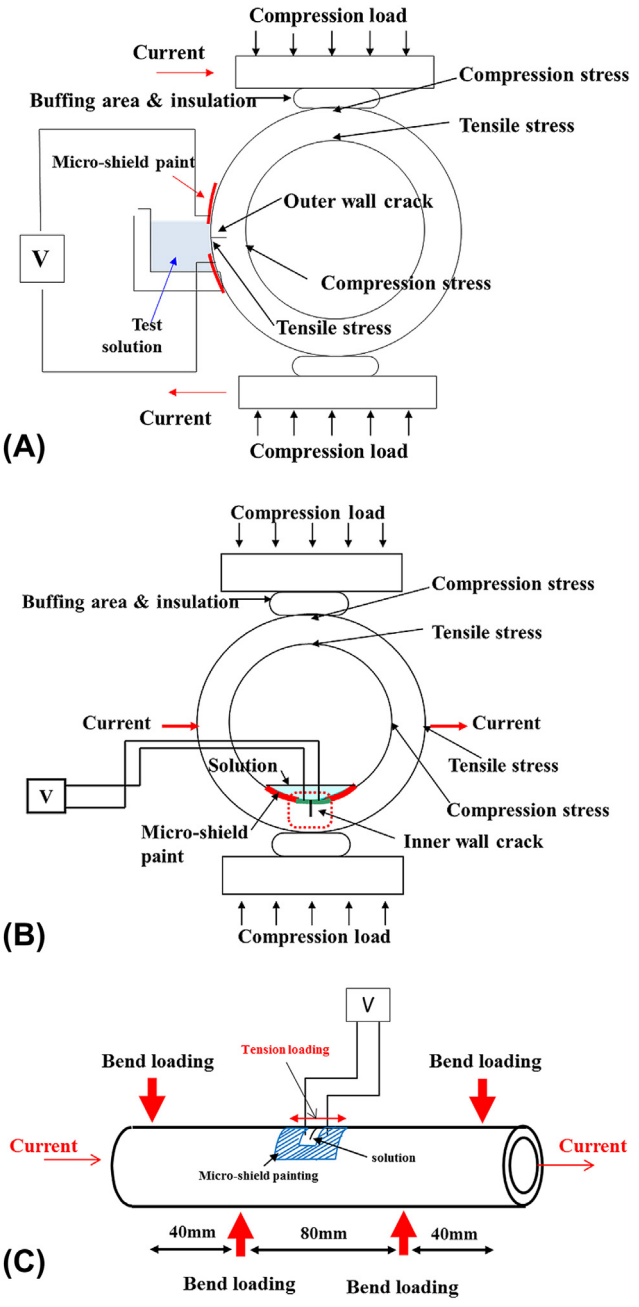

Fig. 2 – Schematics of the radial denting method applied to generate axial cracking at (A) the outer and (B) the inner wall surfaces. (C) Schematic of the axial tension method used for generating circumferential cracks.

opening exposed to the corrosive aqueous conditions. Each DCPD probe was held in contact with the test specimen by a helical spring inside the probe. For outer diameter (OD) cracks in parallel, crack evolution was monitored using the traveling microscope installed in front of the tube.

2.3. *FEA of loading conditions*

Elastic-plastic FEA calculations were performed to predict the stress distribution and plastic deformation at the optimum

loading conditions, which were based on analyses of the characteristics of defects in alloy 600 base and alloy 182 weld metals in NPP components. Radial-denting and four-point–bending methods were applied to produce axial and circumferential cracks respectively in the tubular specimens. These methods have been demonstrated to generate mock-up cracks with high aspect ratios, i.e., crack length/depth ratios, like those typically obtained in NPP components. The loading schemes used in this study have the advantage of using on-line crack monitoring, which allows easier prediction of the location of stress concentration [14].

2.4. *Measurement of mock-up cracks*

To control and monitor the initiation and propagation of mock-up cracks, an online DCPD method was developed. This method enables reproducible production of mock-up cracks that have the target geometries. Using array probes, the electrical potential differences were measured along the crack length at several positions in the specimens. The accuracy of the crack length and depth measurements was assessed by comparing the DCPD measurement results with those of an electrostatic FEA simulation. This enables the derivation of a calibration equation that describes the relationship between the measured electrical potential drop signal and the crack depth and length.

The electrostatic FEA simulations, created using ANSYS commercial FE software, were used to model the DC potential drop, with the increase in crack depth for both the alloy 600 base metal and the alloy 182 weld metal. FE meshes with two-fold symmetry and potential distribution contours for specimens with and without a crack were constructed. A constant direct current of 5 A was applied to the PZR heater sleeve nozzle specimen, and five sets of probe wires were attached at separations of 2 mm across the crack area. The potential drop of the heater sleeve nozzle specimen was calculated assuming that both axial and circumferential cracks increase in stages with fixed $a/c = 0.1$, where a is the crack depth, c is crack length, and a/c is the aspect ratio of the crack. The potential at each probe location was predicted to increase gradually as the crack length (at a fixed aspect ratio) increased.

The analytical results based on the electrostatic FEA simulation were compared with the experimental results to evaluate the validity and applicability of the derived equation, and the final characterization of the mock-up crack was confirmed by destructive metallographic analysis. The reliability of the FEA simulation of DCPD monitoring was confirmed in a previous study on SG tubing materials [14]. The FEA simulation was performed on compact-tension specimens with various sizes of cracks, and the results were compared with Johnson's theoretical equation according to ASTM Method E 1737-96.

2.5. Results and discussion

In total, eight different mock-up cracks in axial and circumferential intergranular stress corrosion configurations on the inner and outer surfaces of the alloy 600 base and alloy 182 weld metals were generated in this study. The final results

Table 2 – The final results obtained for the mock-up cracks created in various geometries and under various environmental conditions.

Material	Crack location	Crack type	Sensitization heat treatment condition	Applied load	Crack length[a] (mm)	Crack length[b] DCPD, (mm)	Error[c] (%)	Max. crack depth[a] (%TW)	Max. crack depth[b] (%TW)	Error[d] (%)
Alloy 600 base metal	OD	Axial	700°C / 5h	255 kN/m	18.5	15	81	77	50	65
		Circumferential	700°C / 5h	17.5 kN	5.88	8	136	72	48	67
	ID	Axial	700°C / 5h	135 kN/m	16.9	12	71	57	38	67
		Circumferential	700°C / 5h	17.5 kN	6.65	9	135	57	46	81
Alloy 182 weld metal	OD	Axial	SA + SR[e]	179 kN/m	12.4	13	104	90	56	62
		Circumferential	SA + SR	10 kN	5.28	11	208	83	68	82
	ID	Axial	SA + SR	87 kN/m	5.22	–	–	82	–	–
		Circumferential	SA + SR	10 kN	7.73	10	129	90	67	74

DCPD, direct-current potential drop; ID, inner diameter; OD; outer diameter; SA, solution annealing heat treatment at 1,100°C for 24 hours; SR, stress-relief heat treatment at 620°C for 24 hours.

[a] Measured by metallographic fracture surface analysis.

[b] Measured by DCPD.

[c] Defined as the ratio between crack length measured by metallographic fracture surface analysis and one measured by DCPD.

[d] Defined as the ratio between crack depth measured by metallographic fracture surface analysis and one measured by DCPD.

[e] SA: solution annealing heat treatment at 1100 °C for 24 h, SR: stress-relief heat treatment at 620 °C for 24 h.

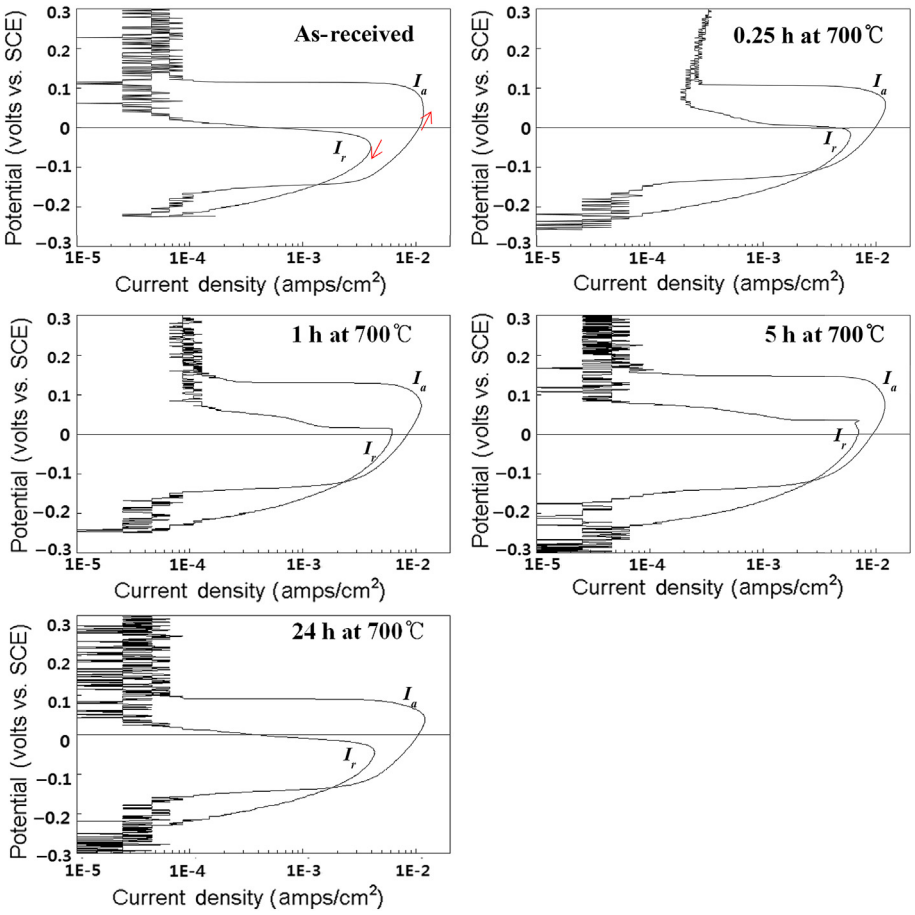

Fig. 3 – Double-loop electrochemical potentiokinetic reactivation results for the heat-treated alloy 600 base metals.

obtained from these mock-ups, including their geometries and sensitization conditions, are summarized in Table 2. The accuracy of the DCPD measurements and the reproducibility of crack generation were confirmed via destructive metallographic analysis. In this section, the detailed results and implementation of the sensitization treatment, FE analysis for loading conditions, online DCPD predictive results, and final production of the mock-up cracks are presented.

Table 3 – Results of the double-loop electrochemical potentiokinetic reactivation test for various sensitization heat treatments of the alloy 600 base metal and the alloy 182 weld metal.

	I_r (A/cm^2)	I_a(A/cm^2)	I_r /I_a [%]
Alloy 600 base metal			
As-received	0.00395	0.0115	34.3
700°C for 0.25 h	0.00596	0.0121	49.3
700°C for 1 h	0.00614	0.0110	55.7
700°C for 5 h	0.00694	0.0119	58.2
700°C for 24 h	0.00428	0.0120	35.8
Alloy 182 weld metal			
As-weld	0.00024	0.0099	2.4
SA (1,100°C for 24 h)	0.00108	0.0114	9.5
SA (1,100°C for 24 h) + SR (620°C for 24 h)	0.00234	0.0103	22.7

SA, solution annealing heat treatment at 1,100°C for 24 hours; SR, stress-relief heat treatment at 620°C for 24 hours.

3.1. *Sensitization heat-treatment analysis*

The results of double-loop EPR testing on heat-treated samples of alloy 600 are shown in Fig. 3. In the data, the peak-current density ratio, I_r/I_a (where I_r is the maximum current density obtained in the reversed reactivation scan and I_a is the critical passivation current density obtained in the forward scan) is used to estimate the degree of sensitization. The analyzed EPR results for all of the sensitization treatments are given in Table 3. The sample, heat treated at 700°C for 5 hours, shows the highest I_r/I_a. Therefore, these conditions were taken to be the most effective for sensitization of the alloy 600 base metals in this study. Orthophosphoric etching generally reveals carbides in the materials, and optical micrographs of the etched alloy 600 materials are shown in Fig. 4. The sample, heat treated at 700°C for 5 hours, showed a larger number of intergranular carbides distributed along the grain boundary than samples treated under different conditions. Based on the results of double-loop EPR testing as well as a microstructural analysis, it was determined that heat treatment at 700°C for

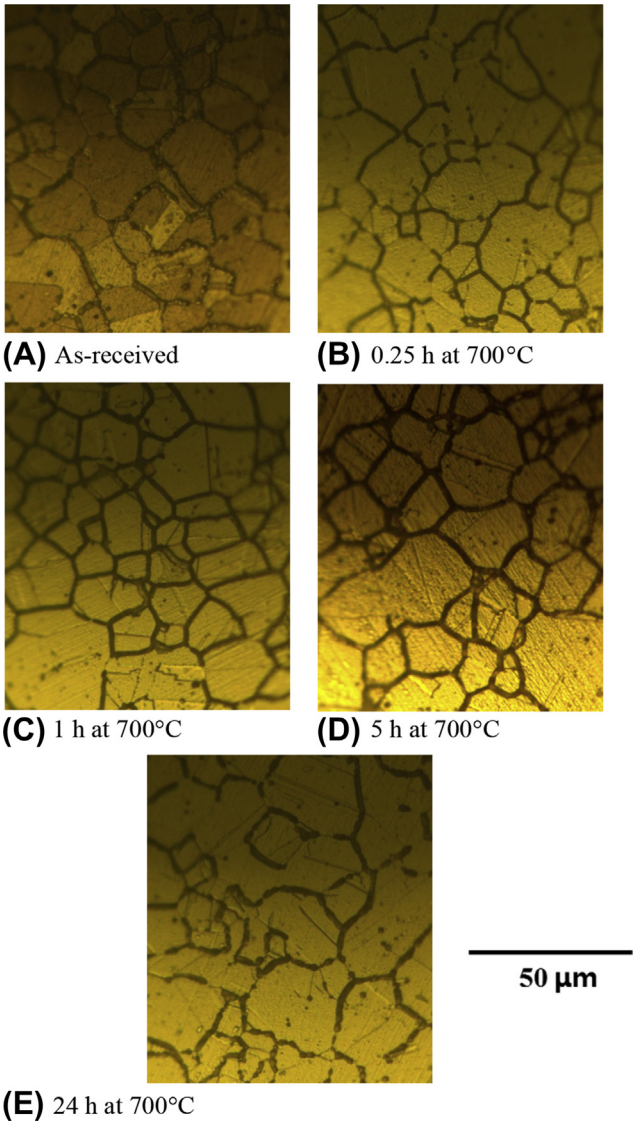

Fig. 4 – Optical micrographs of the heat-treated alloy 600 base metals.

5 hours was most effective for the sensitization of the alloy 600 base metals employed in this study.

The results of the Huey test for the alloy 182 weld showed that the average corrosion rate of a specimen that underwent both SA and SR treatments was 42 g/(m^2•day), while those for the as-welded and SA-treated samples were 9 g/(m^2•day) and 11 g/(m^2•day) respectively. Double-loop EPR tests were performed in the solution containing 0.01M H_2SO_4 + 0.0001M KSCN, and the surface morphology of each specimen was examined microscopically. Fig. 5 and Table 3 show the measured electrochemical potential–current density curves and derived results of the double-loop EPR tests respectively. Fig. 6 shows the results of the microstructural analysis of the heat-treated alloy 182 weld samples. In contrast to the alloy 600 base metals, the alloy 182 weld metals showed a significantly increased corrosion rate after the combined SA + SR heat treatment, as determined via the modified Huey test. The double-loop EPR tests and optical micrographs confirmed that the alloy 182 weld metal was most effectively sensitized by the SA + SR heat treatment; thus, these conditions were adopted to generate mock-up cracks in alloy 182 weld metal in this study.

3.2. *FEA results*

As described previously, the radial denting method was applied to produce a long, shallow axial IGSCC mock-up, while the four-point–bending method was used to produce circumferential IGSCC in the mock-up specimens.

Two- and three-dimensional FEAs using ABAQUS 6.2-1 were performed for the radial denting method in order to confirm the adequacy of the applied stress state. During radial dent loading, tensile stress was induced in the region of the inner wall contacted by the denting jig and the center of the outer wall region respectively. Recent studies [19] have shown that intergranular cracks in sensitized Ni alloys can be produced when a tensile stress corresponding to 90% of yield strength is applied. From the calculated circumferential stress as a function of applied dent load in this study, it is known that dent loadings of 140 kN and 260 kN per meter of axial length are required to reach 90% of the yield strength in order to generate axial inner diameter (ID) and OD IGSCC mock-ups, respectively.

Plastic deformation is also calculated based on the FEA results. Diametric deformation is predicted for loading up to 260 kN/m followed by complete unloading. After unloading completely, the predicted residual plastic deformation is limited to about 6 μm, which is too small to affect the performance of NDE. Therefore, the radial denting method is expected to be suitable to produce axial cracks at the outer and inner walls. The stress and deformation of alloy 600/182 welded piping under dent loading conditions was also analyzed using FEA to determine the optimum loading conditions. It was determined that 179 kN/m and 87 kN/m dent loadings are required to generate axial cracks at the OD and ID of the weld specimens. In the alloy 600/182 weldment, the alloy 182 weld material is sandwiched between alloy 600 base metal regions. Accordingly, the application of stress corresponding to 90% of the yield stress of alloy 182 results in a lower applied stress at the alloy 600 base metal. Therefore, alloy 182 weld mock-up cracks can be generated using lower stress thereby avoiding plastic deformation of the test specimen and base-metal crack generation.

A three-dimensional FEA and solid mechanics analysis were also performed for the 4-point–bend loading conditions to check the adequacy of the stress state and reliability of the tubular specimen design. During application of the bending load, there may be local plastic deformation at the loading point due to the indentation effect depending on the loading method. Therefore, an optimum loading method must be defined before the actual experiments are performed. This analysis was also performed for both the alloy 600 base metal and the alloy 182 weld metal. The optimum loading conditions for alloy 600 base metal were determined first because of its relatively high mechanical strength. Analysis of the weld followed, using the optimized procedure for the base metal. An analytic solution and FEM elastic-plastic analyses were performed in a comparative study to predict the axial stress in

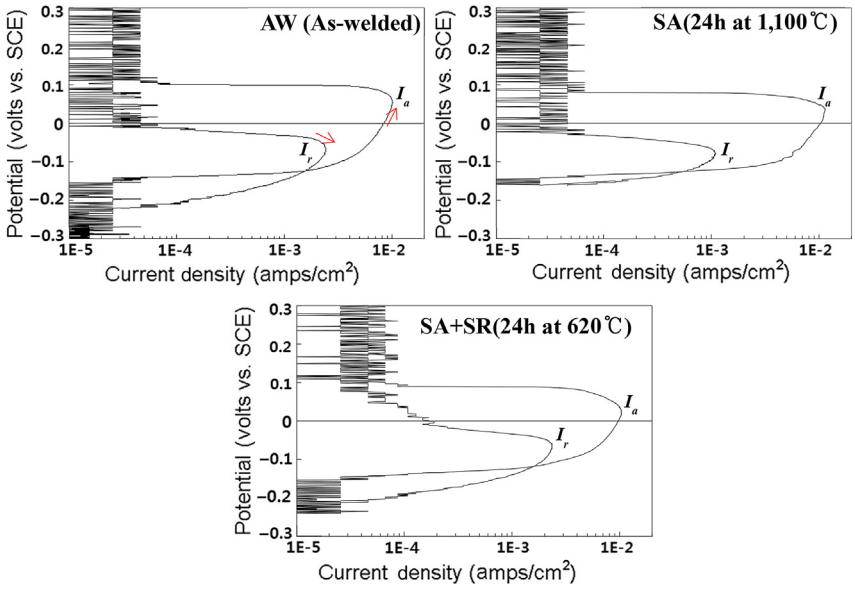

Fig. 5 – Double-loop results for the heat-treated alloy 182 weld metals.

the longitudinal direction of the specimen as a function of bend loading. A line-contact loading method was selected for this study to prevent indentation at the loading point. The results indicate that a bending load of 17.5 kN is required to generate 90% of the yield stress at the cracking zone, and the peak stress occurs at the center of the piping specimen. Also, plastic deformation after complete unloading was limited to a few nanometers, even though point loading was applied. This FE analysis of the four-point–loading method, which was used to generate circumferential cracks, demonstrated its sound mechanical basis. The corresponding results for the alloy 182 weld, obtained using the same procedure as for the base metal, confirmed that optimum stress can be obtained via four-point–bend loading without any plastic deformation.

The predicted potential drop results are summarized in Fig. 7. As shown in Fig. 7A, five pairs of probe wires are

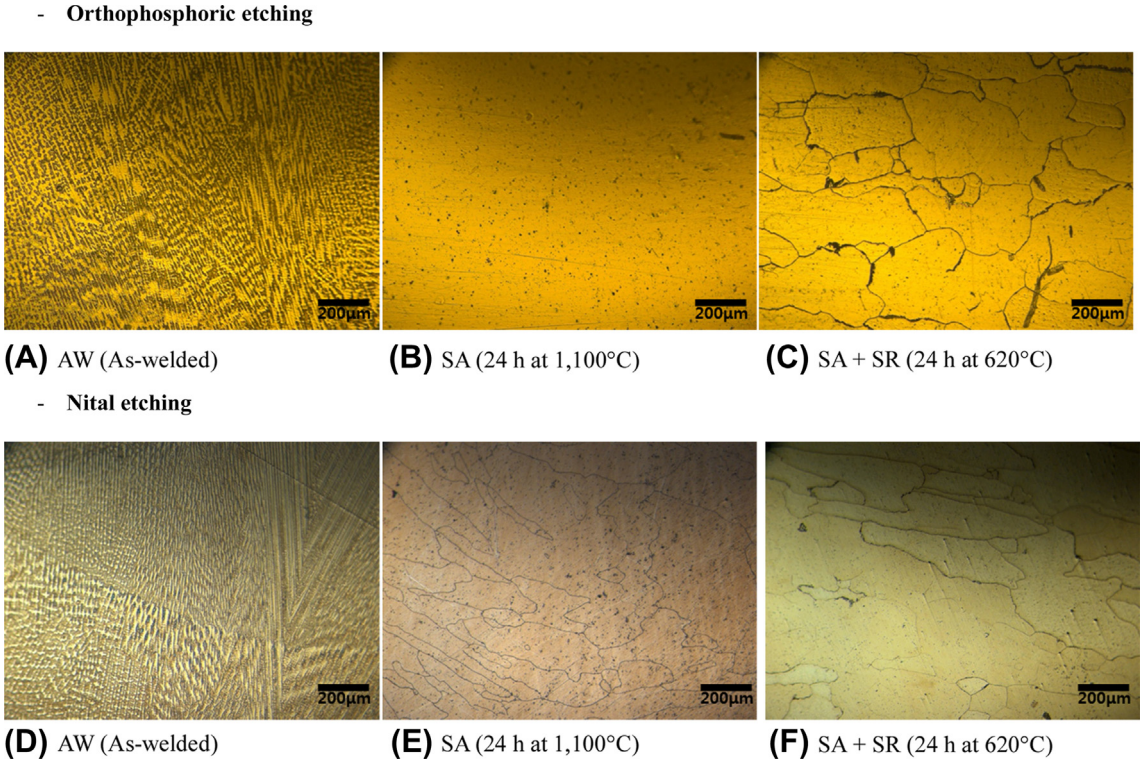

Fig. 6 – Optical micrographs of the heat-treated alloy 182 weld metals. SA, solution annealing heat treatment at 1,100°C for 24 hours; SR, stress-relief heat treatment at 620°C for 24 hours.

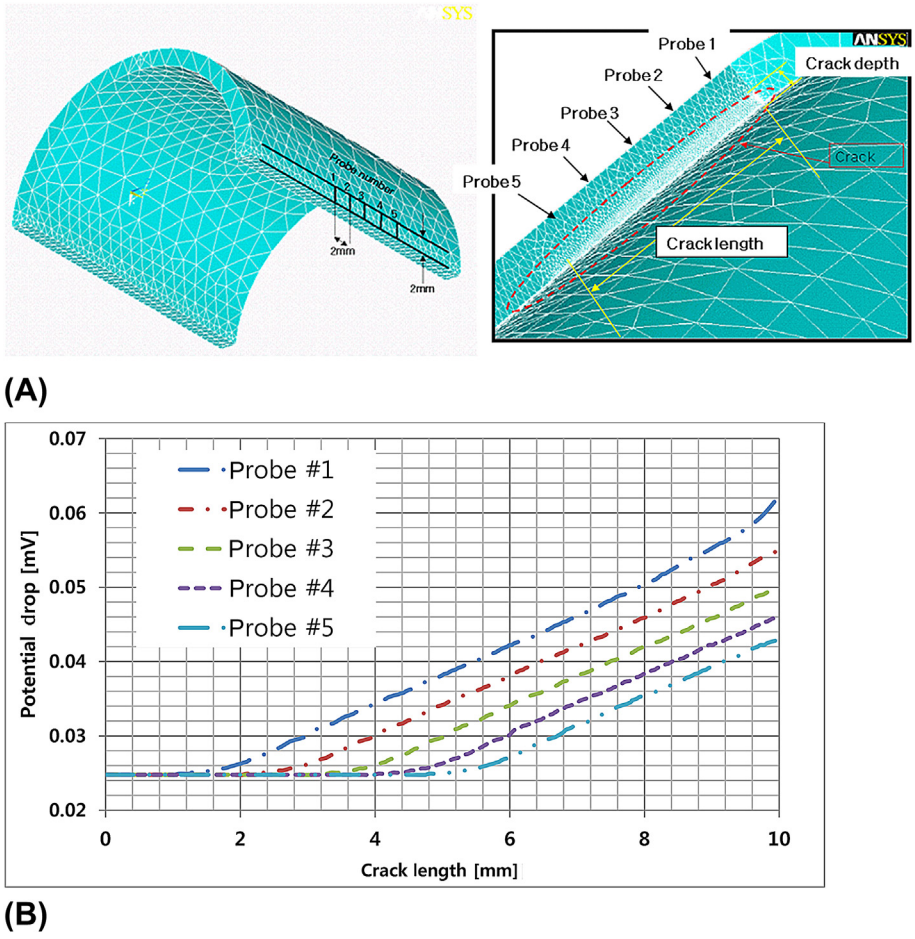

Fig. 7 – (A) The FE model and location of the DCPD probes in the specimen. (B) The predicted DC potential-drop behavior obtained using FEA simulation. DCPD, direct-current potential drop; FEA, finite element analysis.

attached in the cracked region with 2 mm between each pair of probe wires; the location of the first pair of wires is the initiation point of crack in the direction to the next adjacent probe wire. Fig. 7B shows that the DCPD signal was predicted to be about 25 μV without a crack and to increase to 2.5 times the initial value upon the creation and growth of a 1 mm deep crack near the probe location. These FEA simulation results provide the fundamental data required to establish the reproducibility of the mock-up crack specimens via comparison with the empirical data.

The FEA simulation of the DCPD signals is aimed at improving the reliability of DCPD monitoring. This can be accomplished by comparing the simulation data with measured data obtained from the arrayed probes on real experimental specimens. In this section, the DCPD simulation data are verified via comparison with empirical DCPD data for a machined notch specimen. Four different specimens with axial and circumferential cracks on alloy 600 base metal and alloy 182 weld nozzle surfaces respectively, were prepared for this experiment. Electrostatic FEA simulations were performed on the cracked specimens, and DCPD signals were measured under the same conditions for a real crack-production experiment. The results of these analyses on axial and circumferential cracks of alloy 600 and alloy 182 are summarized in Fig. 8. In each graph, the lines with triangles represent the real depth profile of a machined notch specimen, the broken lines show the depth predicted by FEA simulation, and the lines with squares depict the converted crack depths obtained from the measured DCPD signal, which have an error range 25–60% of the real crack size. However, the error of the DCPD measured depth can be reduced to 5–30% when the values are compensated by the consideration that DCPD FEA tends to underestimate the real crack depth by about 30%. The crack-length results were accurately predicted, and the crack shape results were very close to the actual crack geometries.

3.3. *Mock-up crack production in a forged tube of alloy 600 base metal*

Fig. 9 shows the IGSCC produced in the alloy 600 base metal. The dimensions of forged tubes are 29.5 mm in outer diameter and 3.3 mm in thickness. The OD and axial IGSCCs had cross-sectional characteristics typical of an intergranular stress corrosion crack, as shown in Fig. 9A, and the final crack length and depth, as measured by metallographic fracture surface analysis, were 18.5 mm and 2.54 mm (i.e., 77% of the wall thickness) respectively. The

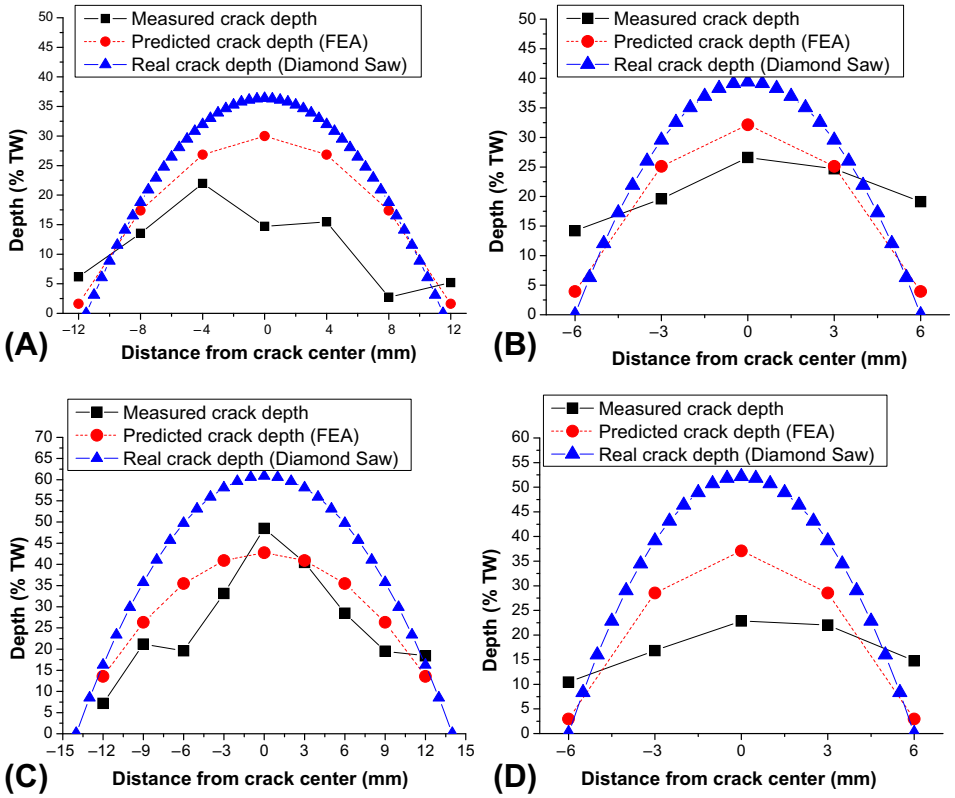

Fig. 8 – Comparative analyses of the various alloy/crack configuration combinations for the verification of the direct-current potential drop method. (A) Alloy 600 base metal axial crack. (B) Alloy 600 base metal circumferential crack. (C) Alloy 182 weld metal axial crack. (D) Alloy 182 weld metal circumferential crack.

length of the OD crack, which could also be measured using the traveling microscope, was predicted to be 15 mm using the DCPD method. The electrical potential drop was measured at five fixed positions via the arrayed probe. The DCPD method was also applied to monitor the crack depth. The maximum depth of the crack, as estimated by DCPD, is 50% of the wall thickness. Therefore, the DCPD method was found to underestimate the crack length and depth by 81% and 65% respectively, compared to the values obtained via metallographic fracture surface analysis.

The results of the characterization of the alloy 600 base metal OD circumferential IGSCC and its comparison with real crack geometry are shown in Fig. 9B. The derivation procedure is the same as that for the axial crack case described previously. The cross-sectional surface features of the produced circumferential crack are also typical of IGSCCs, and the final predicted crack length is overestimated by 36% compared to the real crack length of 5.88 mm. The crack depth is underestimated to a maximum error of 34%. Overall, the predicted shape of the crack is very similar to that of the real crack. It is believed that the differences between the measured and estimated crack sizes originated from the difference between the size of the coverage region of the DCPD probe wires and the actual crack size determined in this study.

During ID crack generation, the online monitoring method plays a more important role in the reproducibility and control of the crack shape because it is difficult to determine whether a crack is produced or not by optical monitoring. The DCPD monitoring method was also applied for this reason, and its feasibility was confirmed through the mock-up crack production experiment. The results are summarized in Fig. 9C. The produced ID axial crack also shows the typical features of IGSCCs with errors of 29% in the predicted crack length and 33% in predicted maximum crack depth. Because the ID axial crack was generated a small distance away from the DCPD probe locations, there is some error in the crack length prediction. Regardless, it is possible to determine when a crack forms.

The final result of the alloy 600 base metal mock-up crack production showed that an ID circumferential crack of the penetration nozzle base metal was successfully produced. The ID circumferential IGSCC mock-up indicated that two semi-circular cracks form and combine with each other, as shown in Fig. 9D. This was also evident from the two crack initiation signals obtained from DCPD that were obtained at separate points. The crack was an IGSCC with a length of 6.65 mm and maximum depth of 1.88 mm. The predicted results from the cracking monitoring were 35% higher than the actual crack length and 20% lower than the actual maximum crack depth.

3.4. *Mock-up crack production in a forged tube of alloy 182 weld metal*

Fig. 10 shows the IGSCC produced in the alloy 182 weld metal of a PZR heater sleeve nozzle. The results of the produced alloy

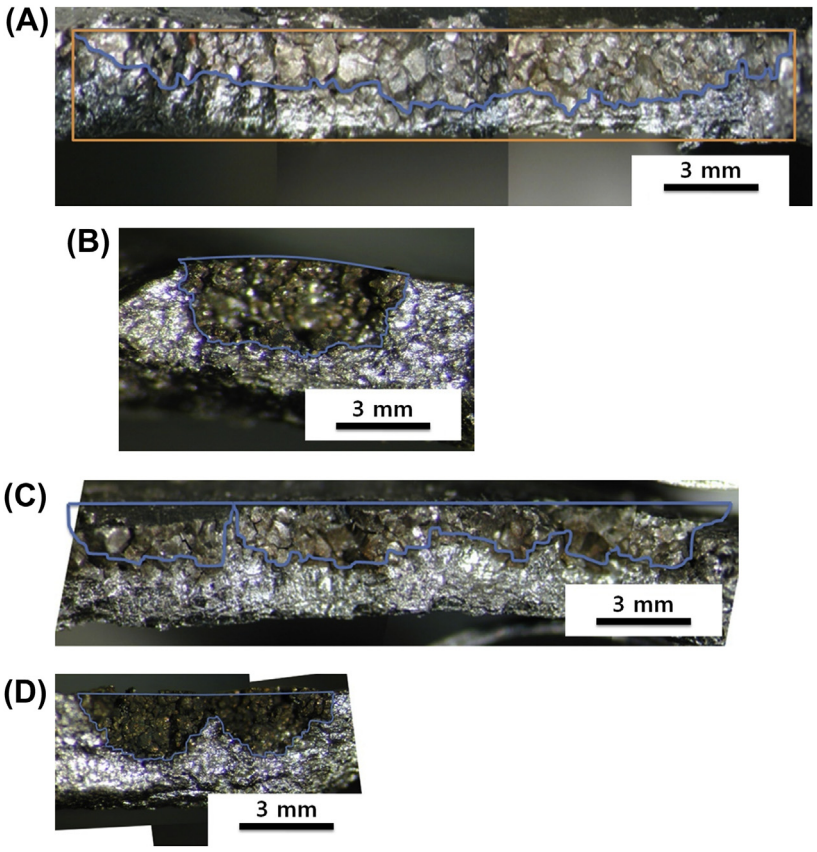

Fig. 9 – Optical micrographs of mock-up cracks generated in the alloy 600 base metal of a PZR heater sleeve. The lines in blue indicate the cracked area produced in this study. (A) OD axial crack. (B) OD circumferential crack. (C) ID axial crack. (D) ID circumferential crack. ID, inner diameter; OD; outer diameter.

182 weld metal OD and axial IGSCC mock-ups are shown in Fig. 10A. In the weld-metal mock-up crack, the produced cracks were confirmed to be typical IDSCCs, which is a type of stress corrosion crack generated in welds in NPPs. The cracks had lengths of about 12.4 mm and depths of 90% of through-wall thickness. The crack had a high aspect (i.e., length-to-depth) ratio, which is typical of those obtained in NPP weld components. The predicted lengths and depths of the crack were overestimated by 4% and underestimated by 38%, respectively, compared to the real crack dimensions.

The produced OD circumferential crack of the penetration nozzle weld also has features typical of IDSCCs, as shown in Fig. 10B. The crack length tended to be overestimated, and the crack depth underestimated, by DCPD.

The axial mock-up crack formed on the ID of the weld has a final length of 5.22 mm and had a maximum depth of 82% of the through-wall thickness. In the alloy 182 weld metal ID axial mock-up crack, the DCPD monitoring signal could not be obtained because of problems with data acquisition. The results of the cross-sectional surface and depth distribution of the final, produced crack are summarized in Fig. 10C.

The circumferential mock-up crack produced on the ID of the alloy 182 weld metal of a PZR heater sleeve nozzle is shown in Fig. 10D. The mock-up crack had the typical features of an SCC in Ni-alloy welding materials. The final crack length was about 7.73 mm and the maximum crack depth corresponded to 90% of the through-wall thickness of the nozzle specimen. DCPD monitoring resulted in a 29% overestimation of the length and a 26% underestimation of the depth.

Eight types of mock-up specimens were produced in this study. It was confirmed that all of the produced mock-up cracks are good representations of the field crack of NPPs using destructive metallographic analysis on the fracture surface. The crack geometries predicted by DCPD monitoring tended to overestimate the crack length and underestimate the crack depth. However, the predicted general crack shapes and monitoring of crack initiation and propagation via DCPD monitoring were generally reliable.

In conclusion, in this study a technique previously developed to produce artificial intergranular stress corrosion cracks in steam generator tubes was extended to forged, tubular alloy 600 base and alloy 182 weld metals for application in the qualification of NDE methods for welded components. The developed procedure was demonstrated to produce intergranular stress corrosion cracks that are comparable to service-induced cracks in both the base- and weld-metal components of pressurized water reactor pressurizer heater nozzles. (1) Sensitization heat treatment was applied in order to make the original materials more susceptible to stress corrosion cracking. (2) While the heat treatment for 5 hours at 700°C was the most effective for alloy 600 base metals, the solution annealing at 1,100°C for 24 hours

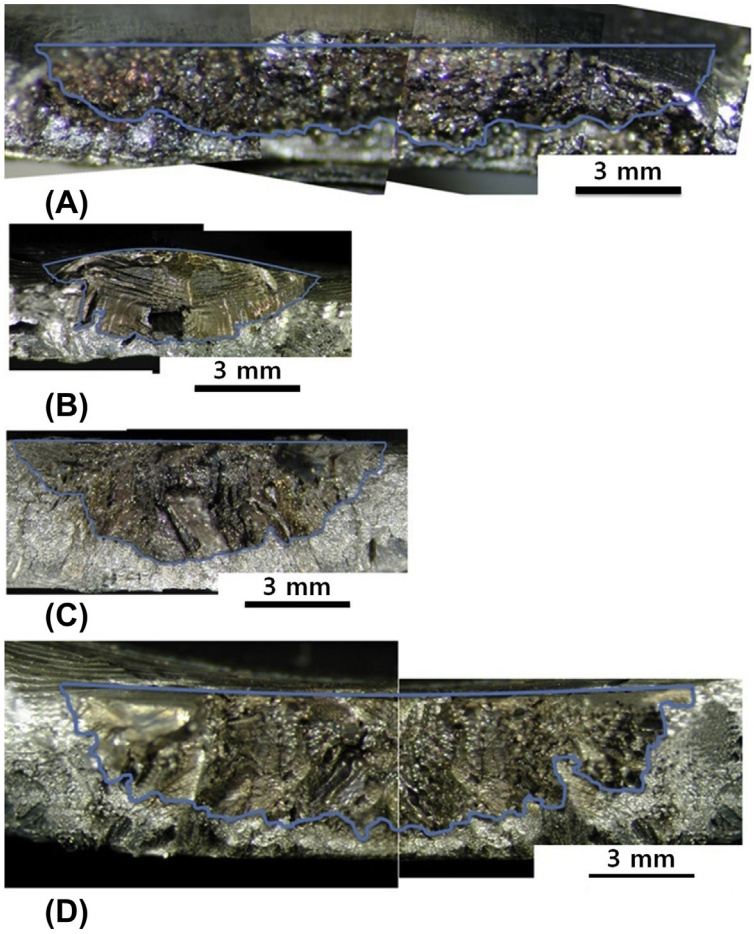

Fig. 10 – Optical micrographs of mock-up cracks generated in the alloy 182 weld metal of a PZR heater sleeve. The lines in blue indicate the cracked area produced in this study. (A) OD axial crack. (B) OD circumferential crack. (C) ID axial crack. (D) ID circumferential crack. ID, inner diameter; OD; outer diameter.

followed by water quenching and stress-relief heat treatment at 620°C for 24 hours and subsequent air cooling was the optimal procedure for sensitization heat treatment for alloy 182 weld metals. (3) Through an FEA, loading conditions to generate optimum stresses of 90% of the yield stress at the cracking zone were determined for radial dent loading and four-point–bend loading without generating any plastic deformation.

An online DCPD method using array probes was applied to measure and monitor the sizes and shapes of cracks during mock-up crack production with high accuracy.

After the tests of mock-up crack production, comparison with destructive metallographic examination demonstrated that the characteristics, orientations, and sizes of the intergranular mock-up cracks produced in this study were highly reproducible using the procedures established.

From the experimental and analytical results obtained by the procedures established in this study, mock-up intergranular cracks in Ni-based forged tubular components, such as PZR heater sleeve nozzles, can be reproduced to a realistic degree, unlike machined notches produced by electro-discharge machining or simple fatigue loading using a universal testing machine. These mock-up cracks provide a useful approach for NDE qualification in nuclear power plants.

Conflicts of interest

All contributing authors declare no conflicts of interest.

Acknowledgments

This work was financially supported by the Nuclear Power Core Technology Development Program (No. 20131520000140, 20131520202310) and International Collaborative Energy Technology R&D Program (No. 20128540010010, 20138530030010) of the Korea Institute of Energy Technology Evaluation and Planning (KETEP), granted financial resource from the Ministry of Trade, Industry & Energy, Republic of Korea.

REFERENCES

[1] D.R. Diercks, W.J. Shack, J. Muscara, Overview of steam generator tube degradation and integrity issues, Nuclear Engineering and Design 194 (1999) 19–30.
[2] J. Wale, Crack Characterisation for In-service Inspection Planning—An Update, SKI Report 2006:24, Swedish Nuclear Power Inspectorate, Stockholm, Sweden, 2006.

[3] D. Straub, M.H. Faber, Modeling dependency in inspection performance, in: 9th International Conference on Applications of Statistics and Probability in Civil Engineering, vol. 2, 2003, pp. 1123–1130. San Francisco, USA.
[4] J.R. Rudlin, L.C. Wolstenholme, Development of statistical probability of detection models using actual trial inspection data, British Journal of Non-Destructive Testing 34 (1992) 583–589.
[5] P.G. Heasler, Piping Inspection Round Robin, NUREG/CR-5068, U.S. Nuclear Regulatory Commission, Washington, DC, 1994.
[6] R. Clark, W.D. Dover, L.J. Bond, The effect of crack closure on the reliability of NDT predictions of crack size, NDT International 20 (1987) 269–275.
[7] I. Virkkunen, M. Kemppainen, J.E. Pitkänen, Effect of Crack Opening on UT Response, in: 9th European Conference on NDT, Berlin, Germany, Th.4.4.2, 2006.
[8] H. Yoneyama, Comparison of echo heights between fatigue crack and EDM notch, Journal of High Pressure Institute of Japan 41 (2003) 115–122.
[9] J.A. Ogilvy, Model for the ultrasonic inspection of rough defects, Ultrasonics 27 (1989) 69–79.
[10] F.L. Becker, C. Latiolais, Experience with inspection qualifications for austenitic piping, Nuclear Engineering and Design 195 (2000) 227–232.
[11] Z. Chen, L. Janousek, N. Yusa, K. Miya, A nondestructive strategy for the distinction of natural fatigue and stress corrosion cracks based on signals from eddy current testing, Journal of Pressure Vessel Technology 129 (2007) 719–728.
[12] M. Kemppainen, I. Virkkunen, J. Pitkänen, K. Hukkanen, H. Hänninen, Production of realistic artificial flaw in inconel 600 safe-end, in: Proceedings of the Conference on Vessel Penetration Inspection, Crack Growth and Repair, Washington D.C., Gaithersburg, USA, 2003, pp. 181–196. NUREG/CP-0191.
[13] M. Kemppainen, I. Virkkunen, J. Pitkänen, K. Hukkanen, H. Hänninen, Advanced flaw production method for in-service inspection qualification mock-ups, Nuclear Engineering and Design 224 (2003) 105–117.
[14] T.H. Lee, I.S. Hwang, H.S. Chung, J.Y. Pak, A new technique for intergranular crack formation in alloy 600 steam generator tubing, Journal of Pressure Vessel Technology 130 (2008) 011403.
[15] I.S. Hwang, S.U. Kwon, J.H. Kim, S.G. Lee, An intraspecimen method for the statistical characterization of stress corrosion crack initiation behavior, Corrosion 57 (2001) 787–793.
[16] R.G. Ballinger, I.S. Hwang, Characterization of Microstructure and IGSCC of Alloy 600 Steam Generator Tubing, EPRI TR-101983, Electric Power Research Institute, Palo Alto, CA, 1993.
[17] W.T. Tsai, C.L. Yu, J.I. Lee, Effect of heat treatment on the sensitization of Alloy 182 weld, Scripta Materialia 53 (2005) 505–509.
[18] T. Kubo, N. Saito, H. Sakamoto, S. Tanaka, Evaluation of sensitization of Ni-base weld metal by the EPR method, in: 10th International Conference on Environment Degradation of Materials in Nuclear Power Systems Water Reactors, Lake Tahoe, Nevada, USA, on CD-ROM, 2001.
[19] D.R. Diercks, W.J. Shack, J. Muscara, Steam Generator Tube Integrity Program, Annual Report, NUREG/CR-6511, vol. 4, U.S. Nuclear Regulatory Commission, Washington, DC, 1999. ANL-98/15.